Journal of Molecular Structure 1196 (2019) 760–770

Contents lists available at ScienceDirect

Journal of Molecular Structure

journal homepage: http://www.elsevier.com/locate/molstruc

Synthesis, structural characterization, Hirshfeld surface analysis, antimicrobial activity, and DNA cleavage studies of (Z)-4-methyl-N'-(phenyl(pyridin-2-yl)methylene)benzenesulfonohydrazide and its Co(II), Ni(II) and Zn(II) complexes

Murat Çınarlı [a], Esra Çınarlı [b], Çiğdem Yüksektepe Ataol [c, *], Önder İdil [d], Ergin Karipta̧ş [e]

[a] Central Research and Application Laboratory, Ahi Evran University, 40100, Kirsehir, Turkey
[b] Department of Biology, Faculty of Science, Ahi Evran University, 40100, Kirsehir, Turkey
[c] Department of Physics, Faculty of Science, Cankiri Karatekin University, 18100, Cankiri, Turkey
[d] Department of Basic Education, Faculty of Education, Amasya University, 05000, Amasya, Turkey
[e] Department of Microbiology, Faculty of Medicine, Ahi Evran University, 40100, Kirsehir, Turkey

ARTICLE INFO

Article history:
Received 19 March 2019
Received in revised form
26 June 2019
Accepted 1 July 2019
Available online 5 July 2019

Keywords:
Sulfonohydrazone
X-ray single crystal
2-Benzoyl pyridine
Metal complexes of sulfonylhydrazone
Hirshfeld surface
DNA bases

ABSTRACT

The NNO tridentate Schiff base ligand of 2-benzoyl pyridine sulfonyl hydrazone **(HL)** and its transition metal complexes [CoL_2] **(1)**, [NiL_2] **(2)** and [ZnL_2] **(3)** have been synthesized and characterized by analytical and spectroscopic studies. The molecular structures of **HL** and [NiL_2] **(2)** have been investigated by X-ray diffraction and DFT/B3LYP methods. Based on the optimized structures, a single point energy calculation was made for **HL** and **(2)** in the different solvent media. The stability of the molecular structures was investigated in different solvent environments by calculating the molecular orbital energies and total energies of the molecular structures. The global reactivity parameters were obtained and the interactions between the molecules with DNA bases such as adenine, cytosine, guanine, and thymine were investigated by using the ECT (electrophilicity-based charge transfer) method and ΔN (charge transfer). Hirshfeld surfaces of **HL** and **(2)** complex were investigated and the interaction energies between the molecules participating in C–H···O/π interactions in the molecular structures were calculated by using the CE-HF energy model. From elemental analysis data, the metal-ligand ratio of the complexes was found to be 1:2. All compounds were examined for their antimicrobial activity against pathogenic microorganisms by the well-diffusion method. DNA cleavage studies of compounds were screened by the agarose gel electrophoresis method. The results showed that complex **(3)** showed highly nicking activity, while **HL**, **(1)** and **(2)** complexes didn't show any nicking activity.

1. Introduction

Schiff base ligands consisting of different donor atoms (eg N, O, S, etc.) show various biological activities and are also important for researchers because they are bound to various metal ions by various methods [1]. These chelating agents are an important class of ligands due to their synthetic flexibility, selectivity, sensitivity toward the central metal atom, and structural similarities with natural biological substances; their importance is ascribed to the presence of an imine group (N = CH–), which helps in elucidating the mechanism of transformation and racemization reactions in biological system [2]. The importance of these ligands depends on their potential uses in catalysis, medicine as antibiotics and anti-inflammatory agents, and in the industry as anti-corrosion agents [3].

Sulfonyl derivatives are well known as antimicrobial compounds. Sulfonyl-hydrazones and sulfonamides, for example, show antibacterial activity against *Staphylococcus aureus* and *Escherichia coli* [4,5]. In the case of sulfonamides, the action mechanism seems to be linked to inhibition of folic acid synthesis, which is essential for bacterial survival [6]. The synthesis of sulfones has drawn much attention over the years because sulfones constitute useful building blocks in natural products and pharmaceutical compounds [7,8]. On the other hand, sulfonyl hydrazones exhibit interesting chemical properties and are useful intermediates in organic synthesis [9–11].

* Corresponding author.
E-mail addresses: yuksektepe.c@karatekin.edu.tr, yuksekc85@gmail.com (Ç.Y. Ataol).

https://doi.org/10.1016/j.molstruc.2019.07.008
0022-2860/

Phenylhydrazone ligands are very versatile in the number of possible metal binding sites they have and, depending on the portion of the ligand involved in the metal complexation, they can act as both bi- and terdentate ligands [12,13]. Phenylhydrazone ligands can be useful molecules to design new molecular materials [14]. The importance of 2-benzoylpyridine metal complexes is due to their availability that facilitates substrate binding, thus stabilizing the reactive intermediates of transition metals [15].

In the present work, (Z)-4-methyl-N'-(phenyl(pyridin-2-yl) methylene)benzenesulfonohydrazide **(HL)** and its Co(II) **(1)**, Ni(II) **(2)** and Zn(II) **(3)** complexes were synthesized. The structures of title compounds have been investigated by using elemental analysis, FTIR and UV-Vis. spectrophotometric methods. The structures of **HL** and diamagnetic [ZnL_2] **(3)** complex were confirmed by ^{1}H NMR. The structures of **HL** and [NiL_2] **(2)** have been investigated by X-ray diffraction method. Hirshfeld surfaces of complexes **HL** and **2** are investigated and the 2D-fingerprint plots of the Hirshfeld surfaces are obtained. In addition to these studies, the molecular structures of the compounds HL and 2 have been optimized using a DFT/B3LYP/6–311G basis set in both gas and solvent environments such as methanol and water. The molecular orbital energies and the global reactivity parameters of these compounds are calculated and also, the interactions between these compounds and DNA bases are determined by using the ECT (electrophilicity-based charge transfer) method and the parameter ΔN (charge transfer). The new compounds were examined for antimicrobial activity against pathogenic strains. DNA binding studies of compounds were screened with pBR322 plasmid DNA.

2. Experimental

2.1. Materials

All material used in this investigation were purchased from Sigma/Aldrich and used as received. All chemicals purchased from commercial suppliers were of reagent grade and were used without further purification.

2.2. Physical measurements and theoretical methods

The elemental analysis was performed on a Thermo Flash 2000 Elemental Analyser. The electronic absorption spectra of title compounds were recorded at room temperature in DMSO solution on a Thermo Evolution UV-Visible Spectrophotometers working between 200 and 1100 nm. The magnetic moments of the complexes were measured by the Gouy method with an MXl Sherwood Scientific instrument magnet power supply. IR spectra were recorded on Thermo Scientific Nicolet iS10 FT-IR spectrophotometer using ATR. ^{1}H NMR spectra were measured in DMSO-d_6 on an Agilent 600 MHz NMR spectrometer. Starting geometries of the compound were taken from X-ray refinement data for computing procedure. The molecular structures of the compounds in the ground state (in vacuo) were optimized by DFT methods to include correlation corrections with the 6–311G basis set in the gas, methanol and water media. DFT forms hybrid functionals, including B3 [16], which defines the exchange functional as the linear combination of Hartree-Fock, local, and gradient-corrected exchange terms. The B3 hybrid functional was used in combination with the correlation functionals [17]. The Highest Occupied Molecular Orbital (HOMO) and the Lowest Unoccupied Molecular Orbital (LUMO) of the molecules were obtained by single point energy calculation in the Ground State (GS) and gas, methanol and water media by using DFT/B3LYP/6–311G. The global reactivity parameters were evaluated using equations given in the Theoretical section. The molecular structures and DNA bases were optimized and their energies were calculated by using DFT in water media.

All the calculations were performed using Gaussian 09 program [18].

2.3. X-ray crystallography

X-ray diffraction data of **HL** and **2** were collected at room temperature with Bruker APEX-II CCD diffractometer equipped with graphite-monochromated Mo-Kα radiation (λ = 0.71073 Å). The structures were solved by direct methods using SHELXS [19] implemented in the WinGX software system [20] and refined by the full-matrix least-squares procedure on F^2 using SHELXL [21]. All non-hydrogen atoms were easily found from the difference Fourier map and refined anisotropically. All hydrogen atoms were included using a riding model and refined isotropically with CH = 0.93–0.96 Å and NH = 0.86 Å, $U_{iso}(H) = 1.2U_{eq}$ (1.5 for the methyl group) for **HL** and **2**, respectively. Crystallographic data of **HL** and **2**, details of the data collection and structure refinements are listed in Table 1.

2.4. Preparations

2.4.1. Synthesis of *HL*

A solution of p-toluene sulfonyl hydrazide (0.186 g, 1 mmol) in methanol (20 mL) was added dropwise to the hot methanolic solution (20 mL) of the 2-benzoyl pyridine (0.183 g, 11 mmol). The reaction mixture was refluxed with stirring for 6 h and kept at room temperature for slow evaporation. The yellow crystalline compound was filtered and recrystallized with methanol. Yield: 82%, Mp.: 159 °C. Elemental Anal. Found (Calcd.) (%) ($C_{19}H_{17}N_3O_2S$): C: 65.50 (64.95), H: 4.88 (4.84), N: 11.82 (11.86), S: 9.71 (9.11). The chemical structure of **HL** is shown in Scheme 1.

2.4.2. Synthesis of metal complexes (*1*, *2*, and *3*)

The metal complexes were prepared by adding 0.2 mmol equivalents of the appropriate metal acetate salt of {Co(II), Ni(II) and Zn(II)} to a suspension solution of 0.4 mmol equivalents of the ligand in 20 mL. The reaction mixtures were stirred under reflux for 3–4 h. The obtained complexes were filtered, recrystallized from methanol and dried. The [NiL_2] complex was recrystallized from methanol.

[CoL_2] **(1);** Color: Brown, Yield: 78%, Mp(decomp.): 250 °C. Elemental Anal. Found (Calc.) (%) ($C_{38}H_{32}N_6CoO_4S_2$): C: 59.65 (60.08), H: 4.14 (4.21), N: 10.75 (11.06), S: 8.71 (8.43). [NiL_2] **(2);** Light brown crystals, Yield: 78%, Mp(decomp.): 230 °C. Elemental Anal. Found (Calc.) (%) ($C_{38}H_{32}N_6NiO_4S_2$): C: 61.25 (60.88), H: 4.42 (4.21), N: 11.21 (11.07), S: 9.12 (8.43).

[ZnL_2] **(3);** Color: Pale yellow, Yield: 65%, Mp(decomp.): 257 °C. Elemental Anal. Found (Calcd.) (%) ($C_{38}H_{32}N_6ZnO_4S_2$): C: 58.97 (59.57), H: 3.72 (4.17), N: 9.95 (10.97), S: 7.89 (8.36). Chemical structures of complexes are shown in Scheme 1.

2.4.3. Detection of antimicrobial activity

The pathogenic bacterial subcultures chosen were *Enterococcus faecalis* ATCC 29212, *Staphylococcus aureus* ATCC 29213, *Pseudomonas aeruginosa* ATCC 27853, *Escherichia coli* ATCC 25922, *Bacillus cereus* (709) Roma, *Bacillus subtilus* ATCC 6633, *Enterobacter aerogenes* sp., *Listeria monocytogenes 4b* ATCC19115, *Shigella dysenteria type 2* NCTC9363, *A. hydrophila* ATCC 7966. In the title, compounds were examined for their antimicrobial activity by the well-diffusion method. Compounds were kept dry at room temperature and dissolved (100 μg/mL and 200 μg/mL) in DMSO. DMSO was used as both solvent and control. DMSO was found to have no antimicrobial activity against any of the tested organisms. 1% (v/v) of a 24 h broth

Table 1
Crystallograhic data for **HL** and **2.**

Molecules	HL	2
Empirical formula	$C_{19}H_{17}N_3O_2S$	$C_{38}H_{32}N_6NiO_4S_2$
Molecular weight	351.41	759.52
Temperature, T (K)	296	296
Wavelength (Å)	0.71073	0.71073
Crystal system	Monoclinic	Monoclinic
Crystal size (mm^3)	0.11 × 0.14 x 0.20	0.05 × 0.06 x 0.15
Space group	C 2/c	C 2/c
a (Å)	26.498(5)	23.583(2)
b (Å)	8.9857(16)	12.3278(10)
c (Å)	18.961(4)	15.7310(17)
α (°)	90.00	90.00
β (°)	130.274(13)	127.897(6)
γ (°)	90.00	90.00
Volume, V ($Å^3$)	3444.5(13)	3609.0(6)
Z	8	4
Calculated density (Mg m^{-3})	1.355	1.398
μ (mm^{-1})	0.206	0.703
θ Range (°)	2.22–28.07	2.97–24.98
Index ranges	h = −32 → 32, k = −11 → 11, l = −23 → 23	h = −28 → 28, k = −14 → 14, l = −18 → 18
Measured reflections	61354	45752
Independent reflections	3377	3164
Observed reflections, (I > 2σ)	3037	2768
Goodness-of-fit on F^2	1.130	1.372
R_1 indices (I > 2σ)	0.05	0.08
wR_2 indices (I > 2σ)	0.11	0.14
CCDC Number	1830873	1830875

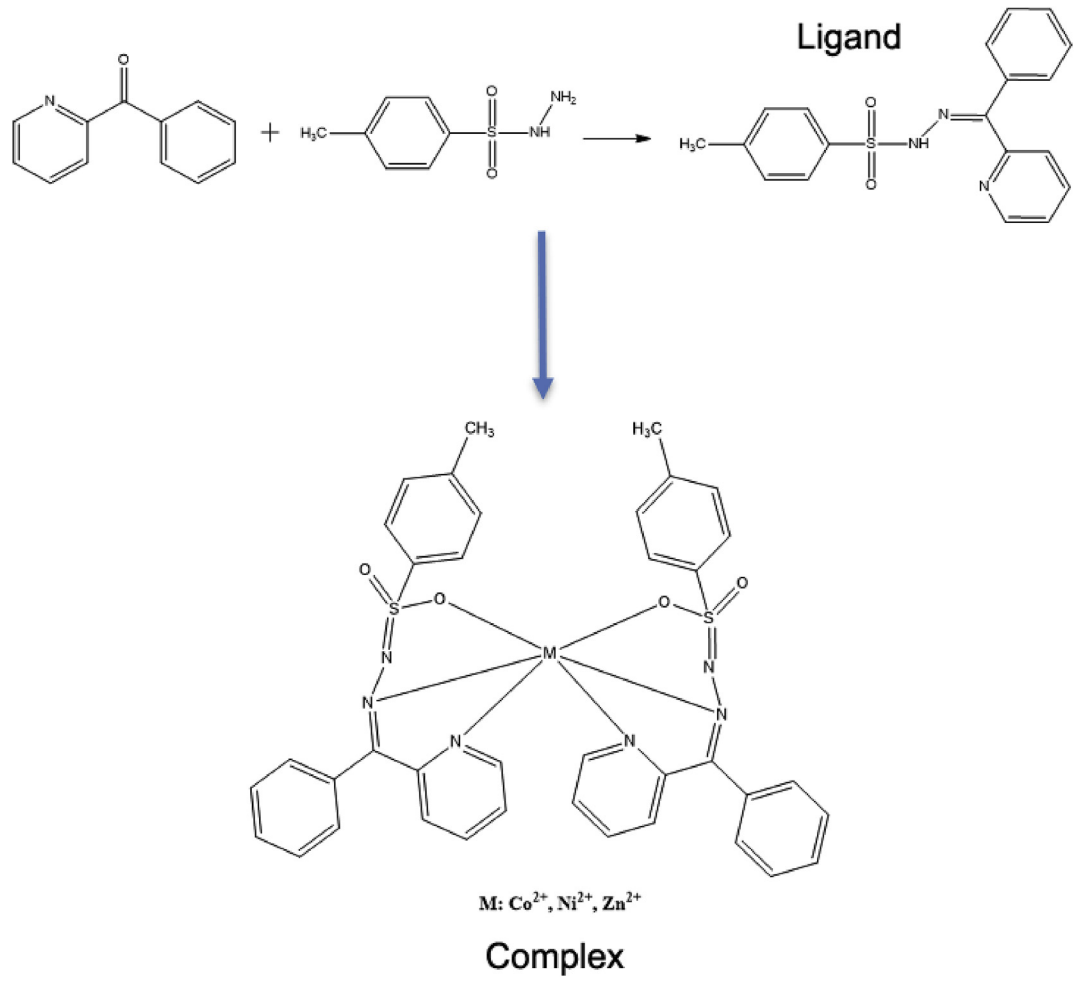

Scheme 1. Synthesis of (**HL**), **1**, **2**, and **3**.

culture containing 10^6 CFU/mL was placed in the sterile Petri dishes. Tryptic Soy Broth (TSB) (15 mL) kept at 45°C was then poured into the Petri-dishes and allowed to solidify. Then wells of 6 mm diameter were punched carefully by using a sterile cork borer and were entirely filled with the test solutions. The plates were incubated for 24 h at 37 °C. On completion of the incubation period, the mean value obtained for the two holes was used to calculate the zone of growth inhibition of each sample.

2.4.4. DNA interaction studies

The cleavage of pBR322 DNA by synthesized compounds was explored via agarose gel electrophoresis. Compounds were prepared in DMSO at 2 mg/mL concentration. pBR322 plasmid DNA (0.25 μg/mL) was treated with each compound and mixture incubated at 37 °C for 4 h. Non treated (H_2O control) and treated with 1 μL of DMSO (DMSO control) pBR322 plasmid DNA were used as the control. After incubation samples were loaded 1% agarose gel and electrophoresis was carried out 120 V for 80 min in TAE buffer (40 mM Tris/acetate and 1 mM EDTA, pH 8.0). The gel was stained in EtBr (1 mg/mL) and the bands were visualized by a UV illuminator. DNA cleavage activity was controlled by relaxation of the super coiled circular form of pBR322 DNA.

3. Result and discussion

3.1. Structure description of (HL) and (2)

The compounds **HL** and **2** are shown in Figs. 1 and 2. The compounds crystallize in monoclinic space group C 2/c. The selected bond parameters for the ligand and its metal complex structure are provided in Table 2. The Ni atom shows an almost octahedral N_4O_2 coordination sphere with the two ligands, meridionally oriented, coordinating the metal ion via the pyridine-N, hydrazone-N and sulfonyl-O atoms [22,23]. In **2**, the pairs of corresponding coordinate bond lengths to the two ligands are almost the same. Similar complexes containing Mn(II), Ni(II), and Zn(II) are reported [24]. The double bond lengths C(20)–N(5) and C(6)–N(2) are agreeable with the literature (1.253(2) and 1.287(3) Å) [25,26]. The deviation from the perfect octahedral environment is evident from the bond angles around the metal center given in S1. As known from Refs. [27–30] the C–S=N–N sulfonohydrazide linkage is non-planar; the torsion angles of **HL** and **2** are −73.17(16)° and −101.2(4)° for C(1)–S(1)–N(1)–N(2), respectively.

As seen from S2, the compound **HL** has intra/intermolecular hydrogen bonds such as C/N–H···O/π, while the compound **2** has C–H···O/π intra/intermolecular hydrogen bonds.

As can be seen from Fig. 3, the intermolecular hydrogen bond for the compound **HL** present between the C(6) atom of the phenyl ring in the (x, y, z) symmetry and the sulfonyl oxygen atom O(2) in the symmetry of (1/2-x, 3/2-y,-z) forms a dimeric structure. This dimeric form is centered at (1/4, 3/4, 0) and characterized by an $R_2^2(10)$ motif ($R_d^a(r)$: R is a ring in the intermolecular hydrogen bond, d is the number of the donor atoms in the ring, a is the number of the acceptor atoms in the ring and r is the number of the total atoms in the ring) [31]. The $R_2^2(10)$ rings formed by hydrogen bond are centered at [n+1/4, k+3/4, l] (n, k, and l are zero or integer). Also, the C(12) and C(13) atoms of the pyridine ring in the (x, y, z) symmetry form the intermolecular hydrogen bond with the sulfonyl oxygen atom O(1) that the bifurcated acceptor in the symmetry (x, 1 + y, z). This hydrogen bond forms a chain in the b direction by combining the dimeric structures. Besides, there is no classic hydrogen bond interaction in compound **2**. The crystal packing of **2** is stabilized by intermolecular C–H … π interactions.

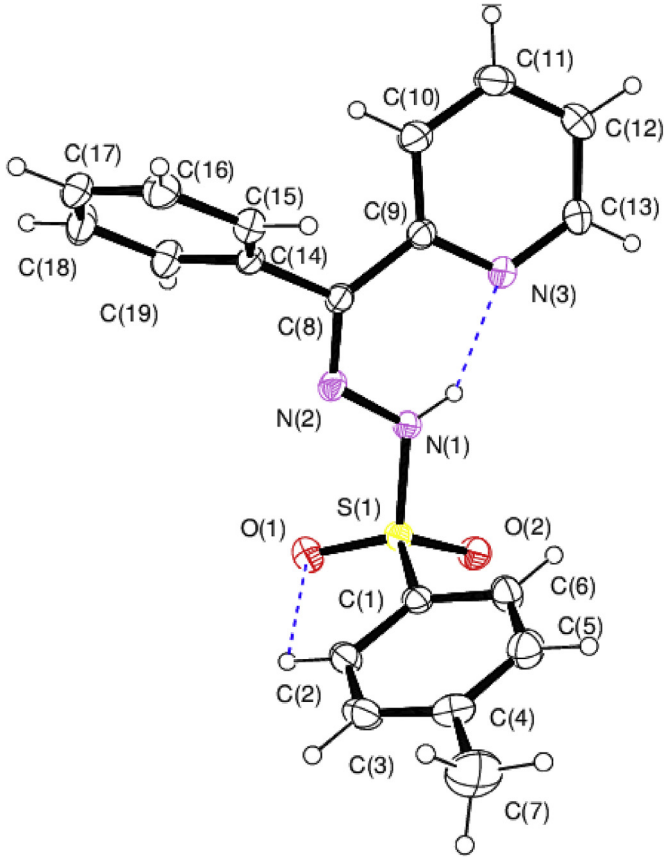

Fig. 1. The molecular structure of **HL**. Anisotropic displacement ellipsoids are drawn at the 50% probability level.

3.2. Hirshfeld surface of (HL) and (2)

The Hirshfeld surface [32,33] of a molecule in a crystal consists of partitioning space in the crystal into regions where the electron distribution of a sum of spherical atoms for the molecule (the promolecule) dominates the corresponding sum over the crystal (the procrystal). Following Hirshfeld [34], we define a molecular weight function $w(\mathbf{r})$:

$$w(r) = \frac{\rho_{promolecule}(r)}{\rho_{prpcrystal}(r)} \quad (1)$$

$$w(r) = \frac{\sum_{A \in molecule} \rho_A(r)}{\sum_{A \in crystal} \rho_A(r)} \quad (2)$$

$\rho_A(r)$, is a spherically-averaged atomic electron density centered on nucleus A, and the promolecule and procrystal are summed over the atoms belonging to the molecule and to the crystal, respectively. The Hirshfeld surface is then defined in a crystal as that region around a molecule where $w(r) \geq 0.5$. That is the region where the promolecule contribution to the procrystal electron density exceeds that from all other molecules in the crystal. The simplest and most immediately useful properties to map onto the surface are the distance from the surface to the nearest nucleus external/internal to the surface, which we call d_e/d_i, respectively. Also, d_{norm} is a normalized contact distance. d_i is normalized by the van der Waals radius of the atom involved; d_e is similarly normalized, and

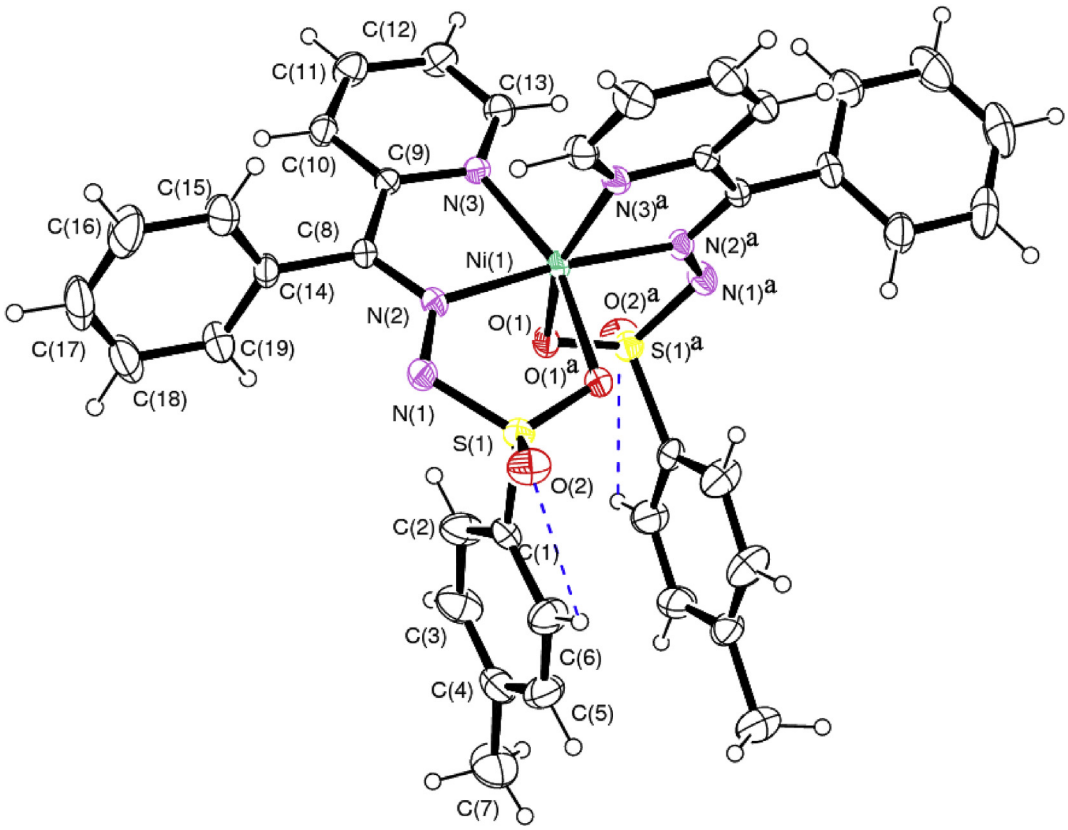

Fig. 2. The molecular structure of **2**. Anisotropic displacement ellipsoids are drawn at the 50% probability level (Symmetry code: (a) -x, y, 1/2-z).

Table 2
The scaled total energies of the interactions between the molecules. R is the distance between molecular centroids (mean atomic position in Å). The scaled total energies are sum of the scaled four energy compenents in kJ mol^{-1}.

M	Symop	R	Electron Density	E_{ele}	E_{pol}	E_{dis}	E_{rep}	E_{tot}
HL	x, 1 + y, z	8.99	HF/3–21G	−20.07	−6.05	−19.82	10.30	−35.64
HL	1/2-x, 3/2-y, -z	6.86	HF/3–21G	−39.74	−16.60	−41.72	29.93	−68.13
HL	-x, 1-y, -z	7.19	HF/3–21G	−14.06	−4.17	−56.13	23.60	−50.76
2	x, 1 + y, z	12.33	HF/3–21G	−2.95	−0.72	−39.73	16.54	−26.86

the sum of these two quantities is the d_{norm} property [35–41]:

$$d_{norm} = \frac{d_i - r_i^{vdW}}{r_i^{vdW}} + \frac{d_e - r_e^{vdW}}{r_e^{vdW}} \quad (3)$$

where atoms make intermolecular contacts closer than the sum of their van der Waals radii, these contacts will be highlighted in red on the d_{norm} surface. If the molecules interact with each other, we can give the total interaction energy in terms of components: electrostatic, polarization, dispersion, and exchange-repulsion:

$$E_{tot} = k_{ele}E_{ele} + k_{pol}E_{pol} + k_{dis}E_{dis} + k_{rep}E_{rep} \quad (4)$$

where k is the scale factor and E_{tot} is the total energy.

The intermolecular interactions of the title compounds **HL** and **2** were quantified using Hirshfeld surface analysis. The calculation were made with CrystalExplorer Software [42]. The mapping of d_i, d_e, d_{norm}, shape index and curvedness of **HL** and **2** are shown in Fig. 4a and Fig. 4b, respectively. These intermolecular contacts (C–H…O/π) are highlighted by conventional mapping of d_{norm} on the molecular Hirshfeld surfaces as shown in Fig. 5a and b for **HL** and **2** and the energies of the interaction (E_{tot}) between the molecules were calculated by CE-HF energy model (see Table 2). The interaction energies between the compounds having (x, y, z) and different symmetries were found as −35.64, −68.13, −50.76 and −26.86 kJmol $^{-1}$, respectively for **HL** and **2**.

The red spots on the surface indicate the intercontacts involved in the hydrogen bonds [43]. Further, intercontacts are plotted with fingerprint plots in S3 and S4: Figures show large surfaces for all intercontacts, H···H intercontacts, C···H, O···H, and N···H contacts plot reveals the information of intermolecular hydrogen bonds.

3.3. IR studies of *(HL)-(3)*

The IR spectra of the compounds shows the characteristic absorption bands at 3066, 1578, 1532, 1347 and 1166 cm^{-1} due to ν $(N–H)_{(hydrazinic)}$, ν $(C{=}N)_{azo.}$, ν $(C{=}N)_{pyr.}$, ν_{as} (SO_2) and ν_s (SO_2), respectively (see Fig. 6 and S5). These values are in accord with the previously reported sulfonyl hydrazone [44,45]. The ν(N–H) band of the free ligand is not present in the spectra of the complexes. This result supporting deprotonation of the ligand during coordination [46,47]. The shift of the band due to ν $(C{=}N)_{azo.}$ and ν $(C{=}N)_{pyr.}$ suggesting that $(C{=}N)_{azo.}$ and $(C{=}N)_{pyr.}$ groups are involved in coordination [48]. In addition, the shift of SO_2 bands of IR spectra of

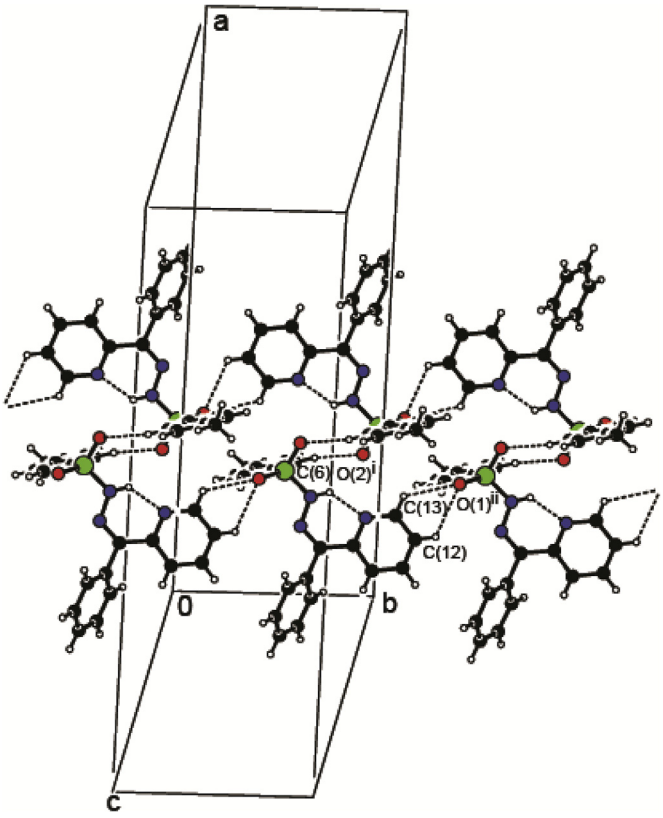

Fig. 3. A partial packing diagram of **HL**, hydrogen bonding interactions have been shown as broken lines. (Symmetry codes: (i) 1/2-x, 3/2-y, -z; (ii) x, 1 + y, z).

the complexes to lower wavelengths indicates that the SO_2 oxygen atom is coordinated to the metal [47]. This coordination behavior of the ligand is also proved by the appearance of IR bands due to n M – O and n M – N vibrations in the range 559–561 cm^{-1} and 430–440 cm^{-1}, respectively [49].

3.4. UV-vis. And magnetic moments studies of (HL)-(3)

The magnetic moment for complex **1** was found to be 3.48 B M. corresponding to high spin ($t_{2g}^5e_g^2$) octahedral configurations. Magnetic moment value of the complex **2** was 2.97 B M., which was in the expected range of octahedral geometry around the central metal ion.

The UV spectra of the **HL** showed two absorption bands at 291 and 294 nm assigned to π–π* transitions of (C=N) and (SO_2) groups, respectively [47]. In the spectra of the complexes, ligand → metal charge transfer bands of **1**, **2**, and **3** were observed at 364 nm ($\varepsilon = 4960$ $Lmol^{-1}cm^{-1}$), 370 nm ($\varepsilon = 4710$ $Lmol^{-1}cm^{-1}$) and 360 nm ($\varepsilon = 2870$ $Lmol^{-1}cm^{-1}$)(see Fig. 7).

Complex **1** exhibits a typical electronic spectra for octahedral structure [50,51]. Two main bands are observed at 564 ($\varepsilon = 182.1$ $Lmol^{-1}cm^{-1}$) and 786 nm ($\varepsilon = 37.5$ $Lmol^{-1}cm^{-1}$), which are assigned to the [$^4T_{1g}(F) \rightarrow {}^4A_{2g}(F)$] and [$^4T_{1g}(F) \rightarrow {}^4T_{2g}(F)$] transitions (see S6).

In the electronic spectra of **3**, one band is observed at 688 nm ($\varepsilon = 37.6$ $Lmol^{-1}cm^{-1}$) in the visible region in DMSO (10^{-2} M) at 25 °C. This absorption band, which is at 688 nm ($\varepsilon = 37.6$ $Lmol^{-1}cm^{-1}$) (see S6).

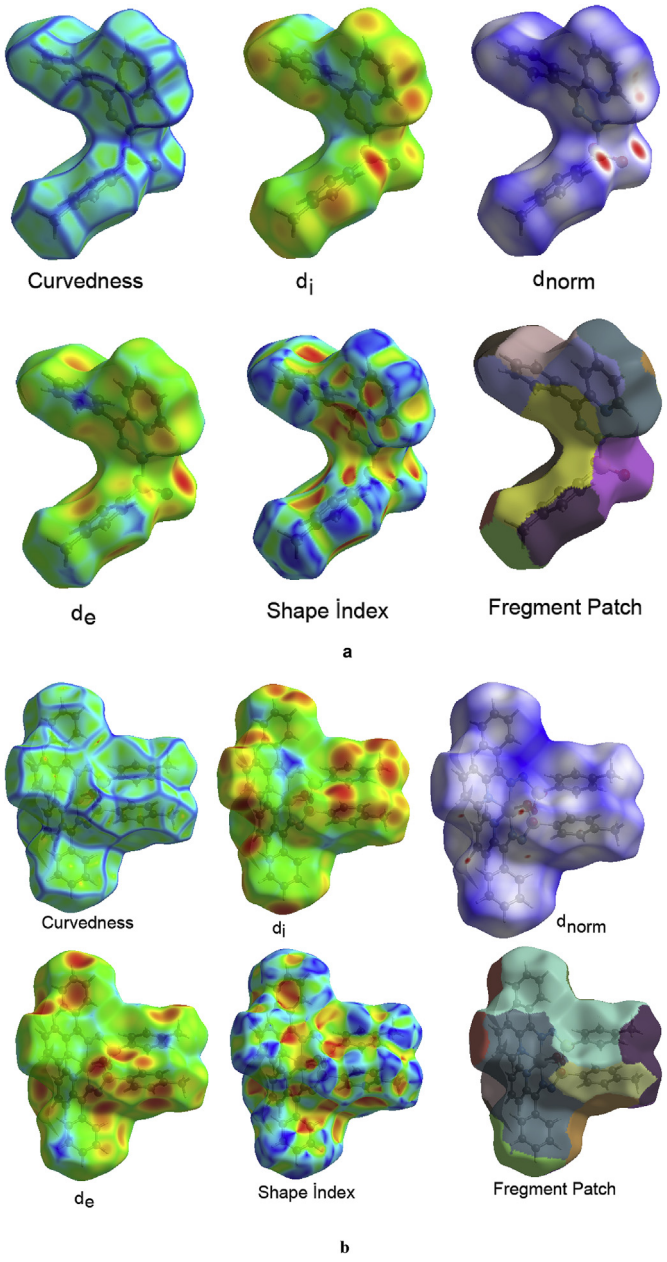

Fig. 4. (a) Curvedness, d_i, d_{norm}, d_e, and shape index for **HL**. (b) Curvedness, d_i, d_{norm}, d_e, and shape index for **2**.

3.5. ^1H NMR studies of (HL) and (3)

^1H NMR spectrum of the ligand (see Fig. 8) in DMSO-d_6 confirmed the proposed structure for **HL**. In ^1H NMR spectra of **HL**, the singlet peak at 11.78 is due to the amidic N–H group. The peak of methyl hydrogen atoms is located at 3.45 ppm and the peaks at 7.28–8.75 ppm are due to the aromatic hydrogen atoms [52,53].

The NMR spectra of complex **3** (see S7) confirmed the coordination of ligand to the metal ion. The NH peak observed in the NMR spectra of the ligand was not observed in complex **4** spectra. The aromatic protons generally appeared around 7.06–8.40 ppm [52].

3.6. Antimicrobial activity of (HL)-(3)

The results obtained from the studies of antimicrobial activity

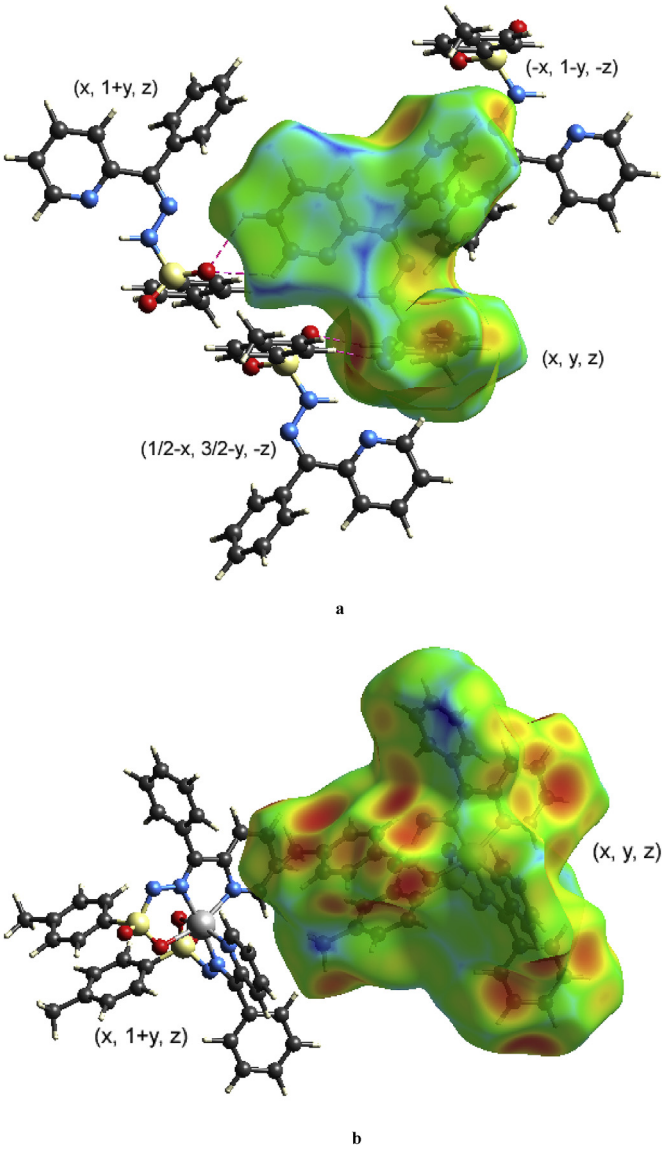

Fig. 5. (a) d_{norm} mapped on Hirshfeld surface for visualizing the intercontacts of the compound **HL**. Dotted red lines represent hydrogen bonds (C (6)–H(6) … O(2)^{i}, C(12)–H(12) … O(1)^{ii}, C(13)–H(13) … O(1)^{ii}, and C(17)–H(17) … Cg(2)^{iii} symmetry codes: (i) 1/2-x, 3/2-y, -z, (ii) x, 1 + y, z, and (iii) −x, 1-y, -z).(b) d_{norm} mapped on Hirshfeld surface for visualizing the intercontacts ofthe compound **2**. Dotted red lines represent hydrogen bonds (C(7)–H(7B) … Cg(5)^{ii} symmetry code: (ii) x, 1 + y, z).

were shown in Table 3. The results show that the compounds are generally active moderately on the bacteria. The most activity for ligand was recorded on *Enterobacter aerogenes* sp bacteria, whereas the most activity for complexes was recorded on *Shigella dysenteria type 2* bacteria. The bacteria in which the compounds were least active were identified as *Bacillus subtilis*. *Aeromonas hydrophila* is a rod-shaped, gram-negative bacterium typical of the aquatic environment that is also found in drinking water, wastewater, sewage, and food. It is considered as an emerging pathogen responsible not only for gastroenteritis and skin infections, but also for more systemic conditions such as peritonitis, bacteremia, meningitis, cholera-like illness, hemolytic uremic syndrome, and necrotizing fasciitis [54–56]. The complex **3** showed high activity on the *Aeromonas hydrophila* bacterium at the concentration of 200 μg/mL. The effect of Zn on microorganisms takes place in two different ways. The first is to increase cell permeability by directly interacting with the cell membrane, causing the cell membrane to become unstable [57]. The lipid membrane, which aids in the passage of lipid-soluble substances, has an important role in controlling antimicrobial activity due to this feature. This increase in lipophilicity, therefore, increases the penetration of compounds into lipid membranes [58]. This limits the further growth of the organism. Newly synthesized Zn complex is thought to have an antimicrobial effect due to this interaction. So it can be said that complex **3** can be used for new drug productions (see S8).

3.7. DNA cleavage studies

There are three DNA forms named supercoiled DNA (Form I), nicked circular DNA (Form II) and linear DNA (Form III).

DNA Cleavage was analyzed by monitoring the conversion of supercoiled DNA (Form I) to nicked circular (NC) DNA (Form II) and linked circular (LC) DNA (Form III) in aerobic condition. When circular plasmid DNA is subjected to electrophoresis, relatively fast migration will be observed for the intact supercoil (SC) form (Form I). If scission occurs on one strand (nicking), the supercoil will relax to generate a slower-moving open circular form (Form II). If both strands are cleaved, an LC form (Form III) that migrates between form I and form II will be generated.

The result of the gel electrophoresis plasmid DNA has two forms, the fast migrating band is the intact supercoil form (Form I) and the slower moving migrating band is the open circular form (Form II), in control groups (Lane 1 and 2). The cleavage efficiency was measured by determining the ability of the complex to convert the super coiled DNA to nicked (open circular) form or sheared form. While ligand, Co complex and Ni complex didn't show any nicking activity, whereas Zn complex showed highly nicking activity [59,60] (Fig. 9). The second effect way of Zn is that Zn ++ ions interact with nucleic acids in prokaryotic cells [61]. It is thought that the synthesized Zn complex is effective on DNA by disrupting the nucleic acid structure. Because it is known that metal complexes convert super-wrapped DNA into open circular DNA [58].

3.8. Theoretical studies using the DFT method

3.8.1. Optimized structures of *(HL)* and *(2)*

The optimized molecular geometries are calculated by using the B3LYP/6–311G method and in the gas, methanol and water media. S9 shows the optimized structures of **HL** and **2** in the gas media. The bond parameters obtained from X-rays and the optimized molecular parameters by B3LYP/6–311G method are comparatively given in S1. Experimental results are the solid phase and theoretical calculations are the gaseous phase [26]. In the solid state, intermolecular interactions connect molecules, resulting in differences in bond parameters between calculated and experimental values. It is well known that DFT optimized geometric parameters are usually good agreement with experimental values and more accurate than Hartree-Fock and semi-empirical methods, due to the inclusion of electron correlation. R^2 (a measure of goodness-of-fit of linear regression) is used the measure of the differences between the calculated and observed values.

As can be seen in S1, the optimized bond lengths and bond angles are the good agreement to the experimental values. According to R^2 values, it can be said that the results obtained in the gas medium are more compatible with experimental bond lengths but the results obtained in the solvent medium are more compatible with experimental bond angles for the compound **HL**, while but the results obtained in the gas environment for both parameters is more compatible with experimental results for the compound **2**. A global comparison was carried out by superimposing the molecular skeletons obtained from the theoretical calculations

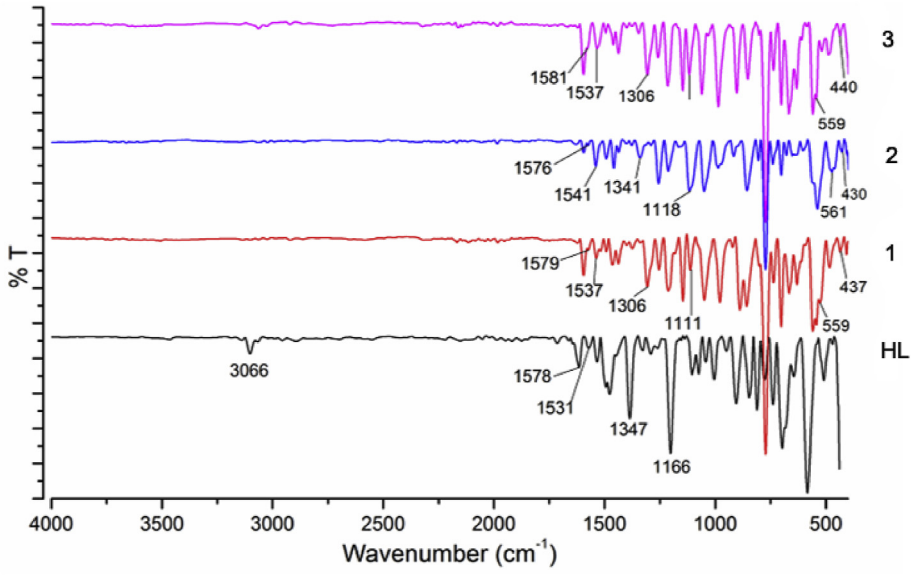

Fig. 6. IR spectra of the compounds.

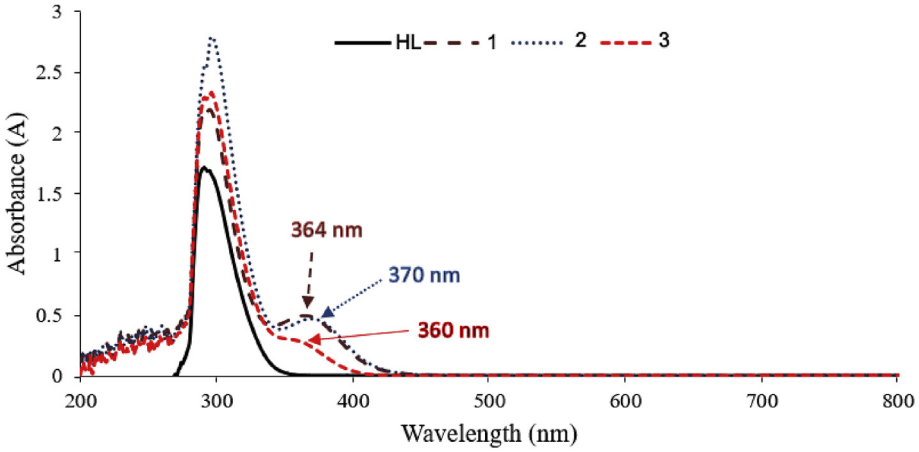

Fig. 7. Absorption spectra of **HL-3** in DMSO 10^{-4} M solution at 25 °C.

and the X-ray diffraction (Fig. 10).

*3.8.2. HOMO and LUMO energies of **(HL)** and **(2)***

A large part of the computational chemistry related to reactivity is based on the concept of the Frontier Molecular Orbitals (FMO), especially the Lowest Unoccupied Molecular Orbital (LUMO) and the Highest Occupied Molecular Orbital (HOMO). The interaction between these orbitals defines the reactivity of reactions [25]. The FMO theory says that attack of an electrophilic species will take place where there is more density of the HOMO, whereas attack of a nucleophilic species will take place in a region with the higher density of the LUMO. The HOMO-LUMO gap (see Fig. 11) and the total energy of the molecular structure are important stability indexes. A low total energy and large band gap of a molecule indicate that it has high stability and low chemical reactivity. This molecular structure is called a hard molecule. In other words, a smaller band gap and higher total energy of a molecule indicate that it has less stability and higher reactivity, and the easier the electron transition will be. This molecular structure is called a soft molecule [62]. In this study, we investigated the effect of solvent groups having different dielectric constant and polarity on E_{HOMO} and E_{LUMO} molecular orbital energies and total energies of the molecular structures. First, the molecular structures (HL and 2) were optimized using the DFT/B3LYP/6–311G method in GS (Ground State) in both gas and methanol and water environments. And then, using optimized structures, the single point energy calculations of molecular structures were performed in the same method and in the same environments. The dielectric constant and dipole moments of the solvents used in the calculations can be given as $\varepsilon = 32.7$, $\mu = 1.7$ D for methanol and $\varepsilon = 80.1$, $\mu = 1.82$ D for water, respectively. Results obtained from solvents having different polarities are shown in S10 and the total energies of the compounds **HL** and **2** were found to be −1446.88735 a.u., −1446.90981 a.u., −1446.91056 a.u., −4400.96521 a.u., −4401.00304 a.u., −4401.00451 a.u. for gas, methanol and water media, respectively. When the energy values obtained from the gas medium and solvent environments are evaluated, we can say that the molecular structures are affected by solvent environments. As a result, the molecular structures have the lowest energy in the water environment, that is, the molecular structures in the water environment are more stable than the other environments. For **HL**, in both solvent media, the structure has the same hardness, but because it has a wide range of HOMO-LUMO for

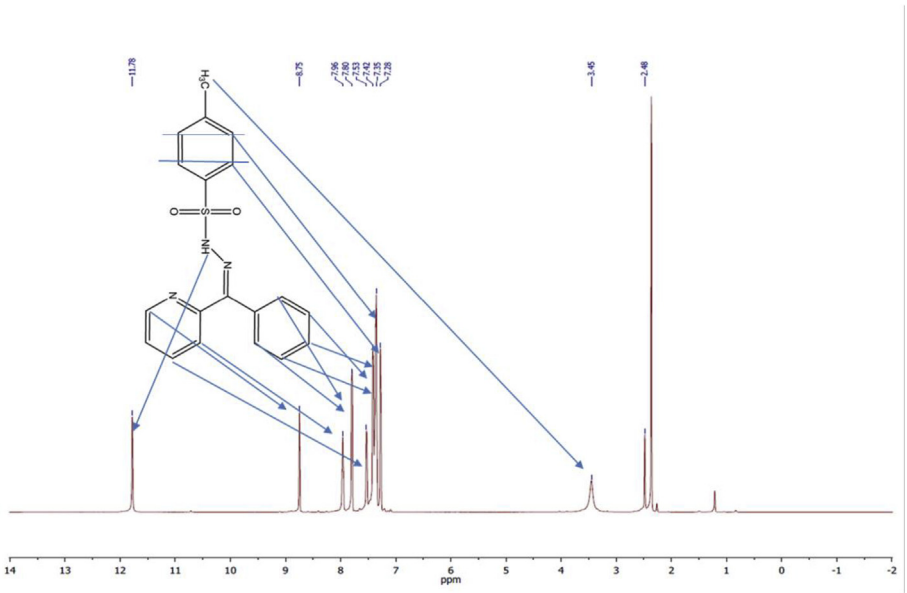

Fig. 8. ^{1}H NMR spectra of HL.

Table 3
Antimicrobial activity of **HL-3** (diameter of zone inhibition (mm)).

Compound	HL		1		2		3		Tetracycline (30 μg)	Trymethoprim (30 μg)
μg/ml	200	100	200	100	200	100	200	100		
Enterococcus faecalis	10	8	8	10	–	12	18	10	27	27
Listeria monocytogenes	15	14	13	15	13	15	18	9		
Pseudomonas aeruginosa	18	12	17	17	15	15	14	15	23	31
Staphylococcus aureus	12	–	12	14	11	14	15	13		
Bacillus cereus	15	16	17	13	13	18	12	14	19	
Enterobacter aerogenes	20	13	13	13	13	12	14	10		28
Bacillus subtilis	13	10	12	10	10	13	12	10	26	20
Aeromonas hydrophila	14	12	15	12	15	16	26	11		
Escherichia coli	14	12	12	13	13	10	14	12	23	
Shigella dysenteria	12	14	12	19	14	18	19	19		

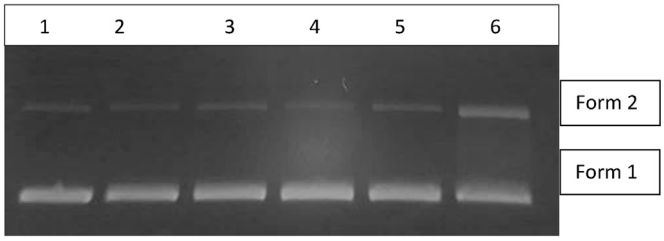

Fig. 9. Lane 1: pBR322 DNA + H_2O, Lane 2: pBR322 DNA + DMSO, Lane 3: pBR322 DNA + Ligand, Lane 4: pBR322 DNA + Co complex, Lane 5: pBR322 DNA + Ni complex, Lane 6: pBR322 DNA + Zn complex.

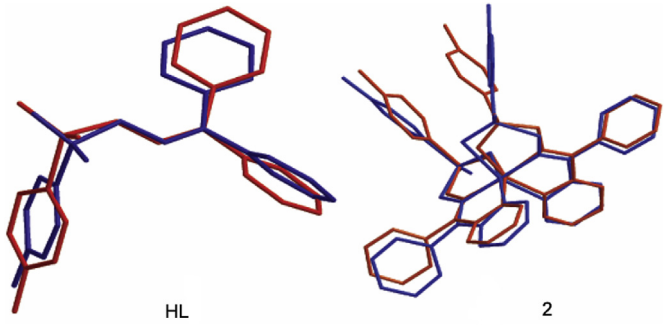

Fig. 10. Atom-by-atom superimposition of the structures calculated (blue) by B3LYP/6–311G (gas) over the X-ray structure (red) for **HL** and **2**. Hydrogen atoms omitted for clarity.

the compound **2**, we can say that it is harder in the water environment.

3.8.3. Global reactivity descriptors of *(HL)* and *(2)*

To investigate the interaction between DNA bases and molecular structures, the molecular structures **HL** and **2** with DNA bases (adenine, cytosine, guanine, and thymine) are optimized by using B3LYP/6−311G method in GS (Ground State) and water media. And then, using the optimized structures, their the single point energies are calculated by B3LYP/6−311G method in water media.

The global reactivity parameters of a molecule are derived from the HOMO and LUMO energy values of molecular structures. The global reactivity parameters were evaluated using equations given. ECT (electrophilicity-based charge transfer) method and ΔN (charge transfer) parameters were used to determine the interactions between these compounds and DNA bases. According to the Density Functional Theory [63,64], the vertical ionization potential (*IP*) and the electron affinity (*EA*) of the molecule are defined as

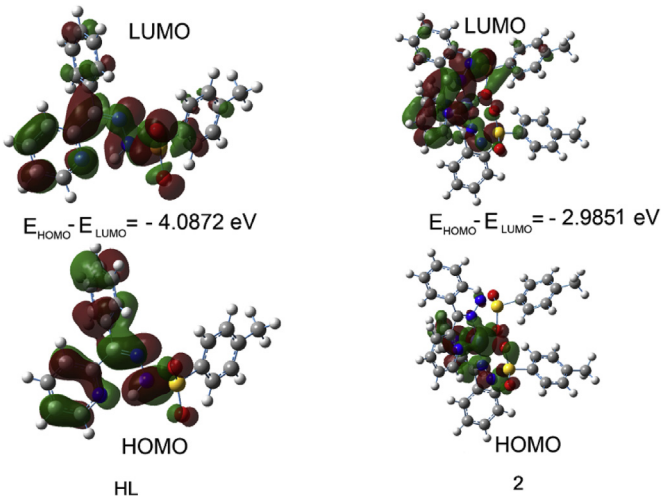

Fig. 11. The HOMO and LUMO energy levels of the molecular structures by DFT/6–311G in methanol media.

$$IP = -E_{HOMO} \tag{5}$$

$$EA = -E_{LUMO} \tag{6}$$

$$\chi = -\mu \tag{7}$$

where E_{LUMO} is the lowest unoccupied molecular orbital's energy and E_{HOMO} is the highest occupied molecular orbital's energy in Eqs. (5) and (6) and χ (eV) in Eq. (7) is the electronegativity. The electronegativity (χ) is equal to the negative value of the chemical potential (μ). In numerical applications, χ and η are calculated using the difference approximation. The electronegativity (χ) and chemical hardness (η) of the molecule are defined as

$$\chi = (1/2)(IP + EA) \tag{8}$$

$$\eta = (1/2)(IP - EA) \tag{9}$$

The electrophilicity index (ω) and global softness (S) are defined as follows:

$$\omega = \frac{\mu^2}{2\eta} \tag{10}$$

$$S = \frac{1}{2\eta} \tag{11}$$

The global interactions between the molecular structure and DNA bases have been determined using the parameter ΔN, which represents the fractional number of electrons, transferred from system A to system B, and is represented by Refs. [65,66].

$$\Delta N = \frac{\mu_B - \mu_A}{2(\eta_A + \eta_B)} \tag{12}$$

where μ_A, μ_B, and η_A, η_B are the chemical potentials and chemical hardnesses of systems A and B, respectively. If $\Delta N < 0$, charge flows from A to B (A acts as an electron donor), and if $\Delta N > 0$, charge flows from B to A (A acts as an electron acceptor). Associated with the definition of global electrophilicity, there is an additional and useful relationship that accounts for the maximum electronic charge ΔN_{max} that the electrophile may accept from the environment. Here, the environment may be represented by either external effects coming, for instance, from the interaction with the solvent or more simply as field effects coming from the presence of substituent groups in the molecule.

ΔN_{max} has been defined as [67].

$$\Delta N_{max} = -\mu/\eta \tag{13}$$

Electrophilicity of a system can be written in terms of ΔN_{max} as follows:

$$\omega = \mu^2/2\eta = (-\mu/2)(-\mu/\eta) = \chi \Delta N_{max}/2 \tag{14}$$

Hence

$$\Delta N_{max} = 2\omega/\chi = 2\omega X \tag{15}$$

where, $X = 1/\chi$.

If we consider the two systems A and B approaching each other, the amount of charge transfer between them can be written in terms of electrophilicity, that is, electrophilicity-based charge transfer (ECT) can be written as

$$ECT = (\Delta N_{max})_A - (\Delta N_{max})_B = 2[\omega_A X_A - \omega_B X_B] \tag{16}$$

If ECT < 0, charge flows from A to B (A acts as an electron donor) and if ECT > 0, charge flows from B to A (A acts as an electron acceptor). It is tacitly assumed that the electrophilicity effect dominates the electronegativity effect.

If the two systems X and Y are brought together, as in a reaction they must form a single system with constant values of chemical potential. The negative chemical potential can be called the absolute electronegativity, and there is always a transfer of electrons from a less electronegative system to a more electronegative system. The amount of charge transfer between the compounds and DNA bases (molecule: B) is calculated based on ΔN and ECT methods to know about the possible interaction of the compounds with the bases (see S10). The values of both ΔN and ECT in S10 indicate that the compounds **HL** and **2** (molecule: A) act as an electron acceptor. In a reaction between two molecules, species can act as a nucleophile (electron donor), which has a lower value of the electrophilicity index. In both methods, while the lowest ECT and ΔN values are found in the interaction between the molecule with the thymine base the largest ECT and ΔN values are found in the interaction between the molecule with the guanine base. When the interactions between DNA bases and molecular structures are examined, we can say that there is a charge transfer from DNA bases to molecular structures.

4. Conclusions

In this study, we reported the synthesis of new sulfonyl hydrazone ligand **HL** and its Co(II) **1**, Ni(II) **2**, and Zn(II) **3** complexes. The structural characterizations of synthesized compounds were made by using the elemental analysis, spectroscopic methods, and magnetic measurements. The structures of **HL** and diamagnetic [ZnL_2] **(3)** complex were confirmed by ^{1}H NMR. The compounds **HL** and **2** have been investigated by X-ray crystallography. X-ray results show that the compounds **HL** and **2** crystallize in space group C 2/c. For both the structures, Hirshfeld surface analysis was carried out. Intermolecular interaction energy calculation results show that the molecule with symmetry (1/2-x, 3/2-y, -z) has a stronger interaction with the symmetric molecule (x, y, z) than the other symmetric structure. This could be because the distance R between the molecular centers is short. Magnetic moment measurements of the

complex structures confirm that the structures have octahedral geometry. ^{1}H NMR spectra of the ligand and complex **3** confirmed the proposed structure for **HL** and the coordination of ligand to the metal ion, respectively. The newly synthesized compounds were found to have moderately antimicrobial activity against bacteria. It has been determined that compounds exhibit the least activity on *Bacillus subtilis*. The complex **3** showed high activity on the *Aeromonas hydrophila* bacterium at the concentration of 200 μg/mL. It has been determined that the only complex **3** showed DNA nicking activity. It is thought that the newly synthesized Zn complex has an antimicrobial effect by interacts with the cell membrane and it is to be effective on DNA by interacting with nucleic acids in the cell. According to the calculation results, we can say that **HL** and **2** are more stable, harder and a low chemical reactivity, high kinetic stability in increasing dielectric constant and dipole moment values solvent environments. And also, we can say that the ligand is harder than the metal complex structure. An electrophilicity-based charge transfer (ECT) descriptor has been proposed in this work. It has been successfully tested on the interaction between the molecular structures **HL** and **2** and DNA bases. ECT shows that the maximum amount of charge transfer takes place between the compounds **HL** and **2** (acts as an acceptor) and guanine (acts as a donor), whereas the minimum amount of charge flows between the compounds **HL** and **2** and thymine and also the compounds **HL** and **2** act as an electrophile (electron acceptor), which has a higher value of the electrophilicity index and the electronegativity value.

Acknowledgments

This work was supported by the Ahi Evran University Scientific Research Projects Coordination Unit. (Project Number: TIP.A4.18.005). The authors acknowledge to Central Research and Application Laboratory, Kırşehir Ahi Evran University. The authors acknowledge to Scientific and Technological Research Application and Research Center, Sinop University, Turkey, for the use of the Bruker D8 QUEST diffractometer.

Appendix A. Supplementary data

Supplementary data to this article can be found online at https://doi.org/10.1016/j.molstruc.2019.07.008.

References

[1] L. Shi, W.J. Mao, H.L. Zhu, J. Coord. Chem. 62 (2009) 3471.
[2] H.A. Saadeh, E.A. Abu Shaireh, I.M. Mosleh, A.G. Al-Bakri, M.S. Mubarak, Med. Chem. Res. 21 (2012) 2969.
[3] A. Budakoti, M. Abid, A. Azam, Eur. J. Med. Chem. 41 (2006) 63.
[4] D.J. Bhatt, G.C. Kamdar, A.R. Parikh, J. Indian Chem. Soc. 2 (1984) 788.
[5] N. Özbek, G. Kavak, Y. Özcan, S. İde, N. Karacan, J. Mol. Struct. 919 (2009) 154.
[6] R.J. Henry, Bacteriol. Rev. 7 (1943) 175.
[7] S.M. Sakya, X. Hou, M.L. Minich, B. Rast, A. Shavnya, K.M.L. DeMello, H. Cheng, J. Li, B.H. Jaynes, D.W. Mann, C.F. Petras, S.B. Seibel, M.L. Haven, Bioorg. Med. Chem. Lett 17 (2007) 1067.
[8] T.K. Sasikumar, L. Qiang, D.A. Burnett, D. Cole, R. Xu, H.M. Li, W.J. Greenlee, J. Clader, L. Zhang, L. Hyde, Bioorg. Med. Chem. Lett 20 (2010) 3632.
[9] W.H. Cheung, S.L. Zheng, W.Y. Yu, G.C. Zhou, C.M. Che, Org. Lett. 5 (2003) 2535.
[10] J.R. Fulton, V.K. Aggarwal, J. de Vicente, Eur. J. Org. Chem. (2005) 1479.
[11] V.K. Aggarwal, J. de Vicente, R.V. Bonnert, Org. Lett. 3 (2001) 2785.
[12] G. García-Herbosa, A. Muñoz, D. Miguel, S. Garcia-Granda, Organometallics 13 (1994) 1775.
[13] A. Bacchi, M. Carcelli, M. Costa, P. Pelagatti, C. Pelizzi, G. Pelizzi, J. Chem. Soc. Dalton Trans. (1996) 4239.
[14] M. Ghedini, I. Aiello, A. Crispini, M. La Deda, J. Chem. Soc. Dalton Trans. (2004) 1386.
[15] R. Beck, U. Florke, H.F. Klein, Inorg. Chim. Acta 362 (2009) 1984.
[16] A.D. Becke, J. Chem. Phys. 98 (1993) 5648.
[17] C. Lee, W. Yang, R.G. Parr, Phys. Rev. B37 (1988) 785.
[18] M.J. Frisch, G.W. Trucks, H.B. Schlegel, G.E. Scuseria, M.A. Robb, J.R. Cheeseman, G. Scalmani, V. Barone, B. Mennucci, G.A. Petersson, H. Nakatsuji, M. Caricato, X. Li, H.P. Hratchian, A.F. Izmaylov, J. Bloino, G. Zheng, J.L. Sonnenberg, M. Hada, M. Ehara, K. Toyota, R. Fukuda, J. Hasegawa, M. Ishida, T. Nakajima, Y. Honda, O. Kitao, H. Nakai, T. Vreven, J.A. Montgomery Jr., J.E. Peralta, F. Ogliaro, M. Bearpark, J.J. Heyd, E. Brothers, K.N. Kudin, V.N. Staroverov, R. Kobayashi, J. Normand, K. Raghavachari, A. Rendell, J.C. Burant, S.S. Iyengar, J. Tomasi, M. Cossi, N. Rega, J.M. Millam, M. Klene, J.E. Knox, J.B. Cross, V. Bakken, C. Adamo, J. Jaramillo, R. Gomperts, R.E. Stratmann, O. Yazyev, A.J. Austin, R. Cammi, C. Pomelli, J.W. Ochterski, R.L. Martin, K. Morokuma, V.G. Zakrzewski, G.A. Voth, P. Salvador, J.J. Dannenberg, S. Dapprich, A.D. Daniels, ∈O. Farkas, J.B. Foresman, J.V. Ortiz, J. Cioslowski, D.J. Fox, Gaussian 09, Gaussian, Inc., Wallingford (CT, USA), 2009.
[19] G.M. Sheldrick, Acta Crystallogr. A71 (2015) 3.
[20] L.J. Farrugia, J. Appl. Crystallogr. 45 (2012) 849.
[21] G.M. Sheldrick, Acta Crystallogr. C71 (2015) 3.
[22] M. Sebastian, V. Arun, P.P. Robinson, P. Leeju, D. Varghese, G. Varsha, K.K.M. Yusuff, J. Coord. Chem. 63 (2010) 307.
[23] N.A. Mangalam, M.R.P. Kurup, Spectrochim. Acta, Part A 78 (2011) 926.
[24] A.S. Pedrares, N. Camina, J. Romero, M.L. Duran, J.A.G. Vazquez, A. Sousa, Polyhedron 27 (2008) 3391.
[25] S. Demir, M. Dinçer, A. Çukurovali, I. Yılmaz, Crystallogr. Rep. 62 (6) (2017) 868.
[26] S.D. Kanmazalp, M. Macit, N. Dege, J. Mol. Struct. 1179 (2019) 181.
[27] N. Şenyüz, Ç.Y. Ataol, H. Bati, Russ. J. Coord. Chem. 40 (11) (2014) 849.
[28] N. Şenyüz, Ç.Y. Ataol, F. Güntepe, H. Bati, M. Taş, R.J., Coord. Chem 42 (6) (2016) 392.
[29] Ç.Y. Ataol, N. Şenyüz, F. Güntepe, M. Taş, H. Bati, Nova Science Publishers, Inc., Chapter of Book, 2017, 978-1-53612-203-9.
[30] M. Çınarlı, Ç.Y. Ataol, H. Bati, F. Güntepe, H. Öğütçü, O. Büyükgüngör, Inorg. Chem. Acta 484 (2019) 87.
[31] A. Zülfikaroğlu, Ç. Yüksektepe, H. Batı, N. Çalışkan, O. Büyükgüngör, J. Struct. Chem. 50 (6) (2009) 1166.
[32] M.A. Spackman, P.G. Byrom, Chem. Phys. Lett. 267 (1997) 215.
[33] J.J. McKinnon, M.A. Spackman, A.S. Mitchell, Acta Crystallogr. B60 (2004) 627.
[34] F.L. Hirshfeld, Their. Chim. Acta44 (1977) 129.
[35] Z. Demircioğlu, Ç. Albayrak, O. Büyükgüngör, J. Mol. Struct. 1166 (2018) 131.
[36] Z. Demircioğlu, G. Kaştaş, Ç.A. Kaştaş, R. Frank, J. Mol. Struct. 1191 (2019) 129.
[37] Z. Demircioğlu, C.C. Ersanli, G.K. Kantar, S. Şaşmaz, J. Mol. Struct. 1181 (2019) 25.
[38] M. Montazerozohori, S. Farokhiyani, A. Masoudiasl, J.M. White, RSC Adv. 6 (2016) 23866.
[39] S. Ghanbari Niyaky, M. Montazerozohori, A. Masoudiasl, J.M. White, J. Mol. Struct. 1131 (2017) 201.
[40] S. Khani, M. Montazerozohori, A. Masoudiasl, J.M. White, J. Mol. Struct. 1153 (2018) 239.
[41] S.M. Jahromi, M. Montazerozohori, A. Masoudiasl, E. Houshyar, S. Joohari, J.M. White, Ultrason. Sonochem. 41 (2018) 590.
[42] M.J. Turner, J.J. McKinnon, S.K. Wolff, D.J. Grimwood, P.R. Spackman, D. Jayatilaka, M.A. Spackman, CrystalExplorer17 (2017).
[43] J.J. McKinnon, D. Jayatilaka, M.A. Spackman, Chem. Commun. (2007) 3814.
[44] N. Karaman, N., Oruc-Emre, E.E., Y. Sıcak, B. Catıkkas, A. Karakucuk-Iyıdogan, M. Öztürk, Med. Chem. Res. 25 (8) (2016) 1590.
[45] M.V. Angelusiu, S.F. Barbuceanu, C. Draghici, G.L. Almajan, Eur. J. Med. Chem. 45 (2010) 2055.
[46] M.A. Ali, A.H. Mirza, M.H.S.A. Hamid, P.V. Bernhardt, O. Atchade, X. Song, G. Eng, L. May, Polyhedron 27 (2008) 977.
[47] J.L. Wang, Y. Jiao, B.S. Yang, Chin. J. Inorg. Chem. 30 (2) (2014) 411.
[48] S.M. Emam, S.A. El-Thana, A. El-Enein, S.M. El-Seady, J. Chin. Chem. Soc. 64 (2017) 261.
[49] Ü.Ö. Özdemir, N. Akkaya, N. Özbek, Inorg. Chim. Acta 400 (2013) 13.
[50] V.P. Daniel, B. Mukuran, B.S. Kumari, K. Mihanan, Spectrochim. Acta, Part A 70 (2008) 403.
[51] E. Vinuelas-Zahinos, M.A. Maldonado-Rogado, F. Luna-Giles, F.J. Barros-Garcia, Polyhedron 27 (2008) 879.
[52] S. Aslkhademi, N. Noshiranzadeh, M.S. Sadjadi, K. Mehrani, N. Farhadyar, Polyhedron 160 (2019) 115.
[53] R. Anbazhagan, K.R. Sankaran, Spectrochim. Acta Mol. Biomol. Spectrosc. 135 (2015) 984.
[54] J.M. Janda, S.L. Abbott, Clin. Microbiol. Rev. 23 (2010) 35.
[55] P. Holmes, L.M. Niccolls, D.P. Sartory, The ecology of mesophilic aeromonas in the aquatic environment, The Genus Aeromonas (1996) 127–150.
[56] P. Brouqui, D. Raoult, Clin. Microbiol. Rev. 14 (2001) 177.
[57] V. Stanic, S. Dimitrijevic, J. Antic-Stankovic, M. Mitric, B. Jokic, I.B.P. Slavica Raicevic, Appl. Sur. Sci. 256 (20) (2010) 6083.
[58] N. Raman, S. Johnson Raja, A. Sakthivel, J. Coord. Chem. 62 (5) (2009) 691.
[59] J. Hong, Y. Jiao, J. Yan, W. He, Z. Guo, L. Zhu, J. Zhang, Inorg. Chim. Acta 363 (2010) 793.
[60] S. Parveen, F. Arjmand, Spectrochim. Acta, Part A 85 (2012) 53.
[61] M. Fang, J.-H. Chen, X.-L. Xu, P.-H. Yang, H.F. Hildebrand, Int. J. Antimicrob. Agents 27 (2006) 513.
[62] M. Çınarlı, Y.A. Çiğdem, M. Taş, H. Batı, J. Mol. Struct. 1169 (2018) 59.
[63] R.G. Pearson, Chemical Hardness: Applications from Molecules to Solids, 1997.
[64] R.G. Parr, W. Yang, Density Functional Theory of Atoms and Molecules, 1989.
[65] R.P. Iczkowski, J.L. Margrave, J. A. Chem. Soc. 83 (1961) 3547.
[66] R.G. Parr, R.G. Pearson, J. A. Chem. Soc. 105 (1983) 7512.
[67] J. Padmanabhan, R. Parthasarathi, V. Subramanian, P.K. Chattaraj, J. Phys. Chem. A 111 (2007) 1358.